VISUAL INFORMATION OF THE MODE FORMATION IN ACCELERATING TAYLOR VORTEX FLOW WITH FINITE LENGTH

H. FURUKAWA[1], T. WATANABE[2] and I. NAKAMURA[3]

Keywords : Formation process, Taylor vortex flow, Non-uniqueness, Non-linear phenomenon

ABSTRACT

As a paradigm of non-linear systems, we numerically study and visualize the Taylor vortex flow between two concentric rotating cylinders with finite length. The governing equations are the unsteady Navier-Stokes equations. The outer cylinder wall and the upper and lower end walls of the cylinders are stationary, and the inner cylinder begins to rotate with a constant accelerations. The main parameters that determine the modes of the Taylor vortex flow are the aspect ratio and the Reynolds number. The former is defined by the ratio of the cylinder length to the gap between cylinders, and the rotation velocity of the representative velocity that is the inner cylinder determines the latter. We have found that, even when the aspect ratio and the Reynolds number are fixed, the final modes of flows depend on the acceleration rate of the inner cylinder. Though the same mode appears under the fixed aspect ratio and the Reynolds number, the developing processes may be different. This indicates that the acceleration rate of the inner cylinder significantly influences the final mode of flows between cylinders.

1 INTRODUCTION

After Benjamin's [1] study, the Taylor vortex flow between two concentric rotating cylinders with finite length has been investigated from various viewpoints. The aspect ratio ? and the Reynolds number *Re* are considered as the main parameters that determine the modes of the Taylor vortex flow [2][3][4]. The aspect ratio ? is defined as the ratio of the cylinder length to the gap between cylinders, and the Reynolds number *Re* is based on the rotation speed of the inner cylinder. Alziary de Roquefort and Grillaud [5] analyzed numerically the Taylor vortex flow by using steady axisymmetric Navier-Stokes equations formulated by the finite difference method. Lücke et al. [6][7] used the unsteady equations, and they reported that Ekman vortices that develop on the stationary end walls cause the bulk Taylor vortex flow when the inner cylinder started to rotate suddenly from rest. Kuo and Ball [8] took the effect of the buoyancy into account and conducted the three dimensional numerical simulation. They found the steady modes in the case that the rotational speed of the inner cylinder was gradually increased from zero. The Taylor vortex flow has a normal mode and an anomalous mode. When the end walls of the cylinders are fixed, the normal mode has a normal cell that gives an inward flow in the region adjacent to the end wall. The anomalous mode has anomalous cell(s) on either or both end walls. The anomalous cell gives an outward flow near the end wall, which is opposite to the flow direction found in the normal mode. Bielek et al. [9] observed experimentally the mode formation processes of the Taylor

Author(s): *1 Nagoya University, Nagoya, 464-8601, Japan, hiroyuki@info.human.nagoya-u.ac.jp*
2 Nagoya University, Nagoya, 464-8603, Japan, watanabe@info.human.nagoya-u.ac.jp
3 Meijo University, Nagoya, 468-8502, Japan, inakamu@meijo-u.ac.jp

Corresponding author: H. Furukawa

vortices, and they have concluded that the anomalous three-cell mode never formed directly after sudden start of the inner cylinder but originated from the decay of the anomalous four-cell mode or the six-cell mode.

One major character of the Taylor vortex flow is its non-uniqueness. The difference of the inner cylinder acceleration rate causes various modes, though the aspect ratio and the Reynolds number are fixed. As mention above, a large number of researches have been carried out into the Taylor vortex flow, but little is known about the non-uniqueness of the mode formation processes of the Taylor vortex flow. The effect of the acceleration rate of the inner cylinder on the mode formation processes has not been reported in detail. When the flow pattern changes, unsteady variations of property values such as torque and kinetic energy arise. The unsteady variation carries the potential for the unexpected system destruction. Therefore, the analysis and prediction of the mode formation processes is important from the engineering viewpoint. In this study, the two-dimensional flow visualization numerically demonstrates the mode formation processes of the Taylor vortex flow between two concentric rotating cylinders. Under the condition that the aspect ratio and the Reynolds number are fixed, the rotation velocity of the inner cylinder is increased from zero at various acceleration rates. The non-unique mode formation processes from the sudden-start of the inner cylinder have also been investigated by us [10].

2 NUMERICAL METHOD

All physical parameters are made dimensionless by using the characteristic length that is the gap between cylinders, the characteristic velocity that is the maximum circumferential rotation speed attained during each calculation, and the characteristic time defined as the ratio of the characteristic length to the characteristic velocity. The governing equations are the unsteady axisymmetric Navier-Stokes equations and the equation of continuity, which are expressed in the cylindrical coordinates (r, θ, z),

$$\nabla\cdot\boldsymbol{u} = 0, \qquad \frac{\partial \boldsymbol{u}}{\partial t} + (\boldsymbol{u}\cdot\nabla)\boldsymbol{u} = -\nabla p + \frac{1}{Re}\nabla^2\boldsymbol{u}, \tag{1}$$

where $\boldsymbol{u}$ is velocity vector with components (u, v, w) in each direction, p is pressure and t is time. Staggered grid is used in this calculation. The number of grid points in the radial direction is 41, and the number of grid points in the axial direction is determined by the proportionality to the cylinder length with 42 points for an aspect ratio of unity. The number of grid points is estimated large enough not to influence results, and the time interval fills the CFL condition. The basic solution procedure is the MAC method, and the time integration is the Euler explicit method. The spatial differentiation is the QUICK method for convection terms and the second-order central difference method for other terms. The inner cylinder is accelerated linearly from zero during the non-dimensional accelerating time T. The initial conditions are that all velocity components are zero in the entire domain. The outer cylinder side, the upper end wall and lower end wall are stationary. The boundary conditions at the cylinder walls and both end walls are no-slip conditions for velocity components, and Neumann conditions for pressure that are obtained from momentum equations. The Stokes stream function ψ is determined as follows, which is used for visualization of the calculated results.

$$u = -\frac{1}{r}\frac{\partial \psi}{\partial z}, \qquad w = \frac{1}{r}\frac{\partial \psi}{\partial r}. \tag{2}$$

To analyze the property of the Taylor vortex flow, we adopt the mean kinetic energy E and the mean enstrophy Ω which are defined by

$$E = \frac{1}{A}\int_S \frac{1}{2}\boldsymbol{u}^2 drdz, \tag{3}$$

T	0.0	8.4	16.8	25.2	33.6	42.0	50.4	58.8	67.2	75.6	84.0
Mode	A4	N2	N2	A4	A4	N4	N4	N2	N4	N4	N4
E	0.07242	0.08427	0.08427	0.07242	0.07242	0.07496	0.07496	0.08427	0.07496	0.07496	0.07496
Ω	0.35060	0.36180	0.36180	0.35060	0.35060	0.42560	0.42560	0.36180	0.42560	0.42560	0.42560

Table 1. Final modes of the Taylor vortex flow (? = 4.0, *Re* = 700).

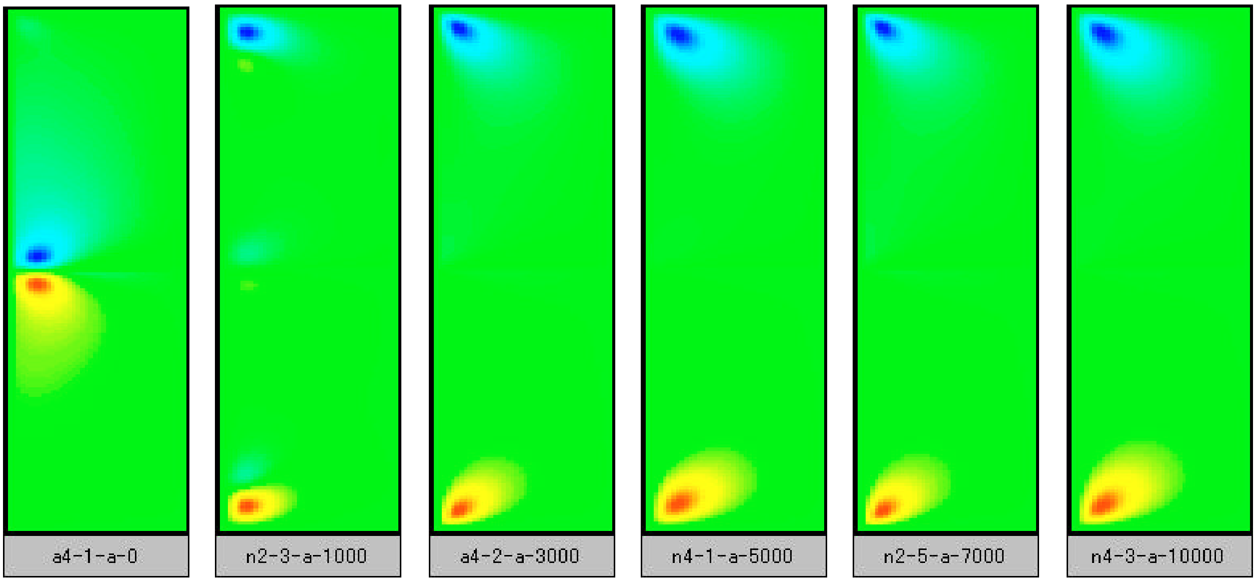

(a) *T* = 0.0 (A4) (b) *T* = 8.4 (N2) (c) *T* = 25.2 (A4) (d) *T* = 42.0 (N4) (e) *T* = 58.8 (N2) (f) *T* = 84.0 (N4)

Fig. 1. Mode formation processes (? = 4.0, *Re* = 700).
Double click each figure, and see animation.

Mode	Process	Mode	Process	Mode	Process
(b) N2 (*T* = 8.4)	N6 →N2	(a) A4 (*T* = 0.0)	N6 →A4	(d) N4 (*T* = 42.0)	N10→N6→N4
(e) N2 (*T* = 58.8)	N10→N2	(c) A4 (*T* = 25.2)	N10→A8→A4	(f) N4 (*T* = 84.0)	N6 →N4

Table 2. The modes formation process of the Taylor vortex flow (? = 4.0, *Re* = 700).

$$\Omega = \frac{1}{2A} \int_S \left(\frac{\partial u}{\partial z} - \frac{\partial w}{\partial r} \right) dr\,dz , \qquad (4)$$

where S is an integral domain and A is the area of a meridional section. We run the calculations 1210 times at ? from 2.6 to 4.6, *Re* from 100 to 1000 and 10 different *T*s.

3 RESULTS

3.1 Mode formation process at ? = 4.0 and *Re* = 700

Table 1 shows the final modes of the Taylor vortex flow at ? = 4.0 and *Re* = 700 in the case that the inner cylinder is accelerated linearly from zero during *T*. Each column of the table indicates the non-dimensional acceleration time *T*, flow mode, the mean kinetic energy *E* and the mean enstrophy ? . Depending on the acceleration time of the inner cylinder, three different modes appear: the anomalous four-cell mode (A4), the normal two-cell mode (N2) and the normal four-cell mode (N4). At the same final mode, the energy E and the enstrophy ? are the same. Table 1 shows that the various modes appear even when ? and Re are fixed. This has been known as the non-uniqueness of the Taylor vortex flow [1].

Figure 1 illustrates the time variations of ψ counters in the (r, z) plane to shows the mode formation processes of the Taylor vortex flow at some Ts. In the figure, the rotating inner cylinder is on the left and the stationary outer cylinder is on the right. The warm color area shows a vortex rotating in a clockwise direction, and a vortex rotating in a counter-clockwise direction is shown cold color area. Figure 1 (a) is the AVI animation that shows the mode formation process of the anomalous four-cell mode. First, two vortices are generated around the mid-plane in the axial direction and they develop in the radial direction. On the other hand, another vortices are formed at the inner-lower and the inner-upper corners. After a while, the flow field becomes the normal six-cell mode. Then, the vortex on the cylinder end wall is pushed aside by the second vortex from the cylinder end wall, and the end-wall cell is divided into two cells: one on the inner cylinder and the other on the outer cylinder. Finally, the boundaries of the interior vortices reach to the cylinder end wall, and the flow field becomes the stable anomalous four-cell mode.

Figure 1 (b) indicates the mode formation process of the normal two-cell mode. The vortices are generated around the mid-plane, and at the inner-lower and the inner-upper corners. Then, the flow field becomes the normal six-cell mode. After a while, the flow field begins to oscillate and it becomes the stable normal two-cell mode after a breakdown of four vortices around the mid-plane.

Figure 1 (c) shows the mode formation process of the anomalous four-cell mode. The vortices are generated around the mid-plane, at the inner-lower and the inner-upper corners, and the transient mode with eight cells is established. Finally, the four vortices around the mid-plane disappear and the flow becomes the stable anomalous four-cell mode.

Figure 1 (d) shows the mode formation process of the normal four-cell mode. The vortices are generated at the inner-lower and the inner-upper corners. First, the normal ten-cell mode is formed. Then, the second vortices from the end walls weaken and disappear. The vortices adjacent to the disappearing vortices rotate in the same direction, and they merge into one vortex. Next, the flow field becomes the normal six-cell mode, and the second vortex and the third vortex from the lower cylinder end wall weaken and disappear. The final mode is the normal four-cell mode.

Figure 1 (e) illustrates the mode formation process of the normal two-cell mode. The vortices are generated around the mid-plane, and at the inner-lower and the inner-upper corners, and the normal ten-cell mode appears. Then, the eight vortices in the interior region disappear, and the flow field becomes the normal two-cell mode.

Figure 1 (f) shows the mode formation process of the normal four-cell mode. The first vortices appear at the inner-lower and the inner-upper corners, and the normal six-cell mode is formed. Then, the flow field begins to oscillate. After a breakdown of the second and third vortices from the lower cylinder end wall, the flow field becomes the stable normal four-cell mode. Table 2 summarizes the mode formation processes shown in Fig. 1.

To determine the number of vortices quantitatively, we use the time variation of the wave number components of the power spectrum of ψ integrated in the radial direction, which is determined by

$$\bar{\psi}(z) = \frac{1}{D}\int_{r_{inner}}^{r_{outer}} \psi \, dr, \qquad S_k = \left| \frac{1}{L}\int_0^L \bar{\psi}(z) e^{-ik\frac{2\pi}{L}z} dz \right|^2, \quad (k = 0, \pm 1, \pm 2, \cdots) \tag{5}$$

where D is the gap length between cylinders and L is the cylinder length. When the component at wave number k is dominant, the flow field has $2k$ vortices. The time variations of S_k are shown in Fig. 2.

Figure 2 (a) indicates the variation in the mode formation process of the anomalous four-cell mode. The dominant wave number shifts from 2 via 3 to 2, and the flow mode is established about t = 40. From this point, we can conclude quantitatively that the final flow field has four vortices. The power spectrum helps us to count the number of vortices, and we can investigate the mode formation processes in more detail.

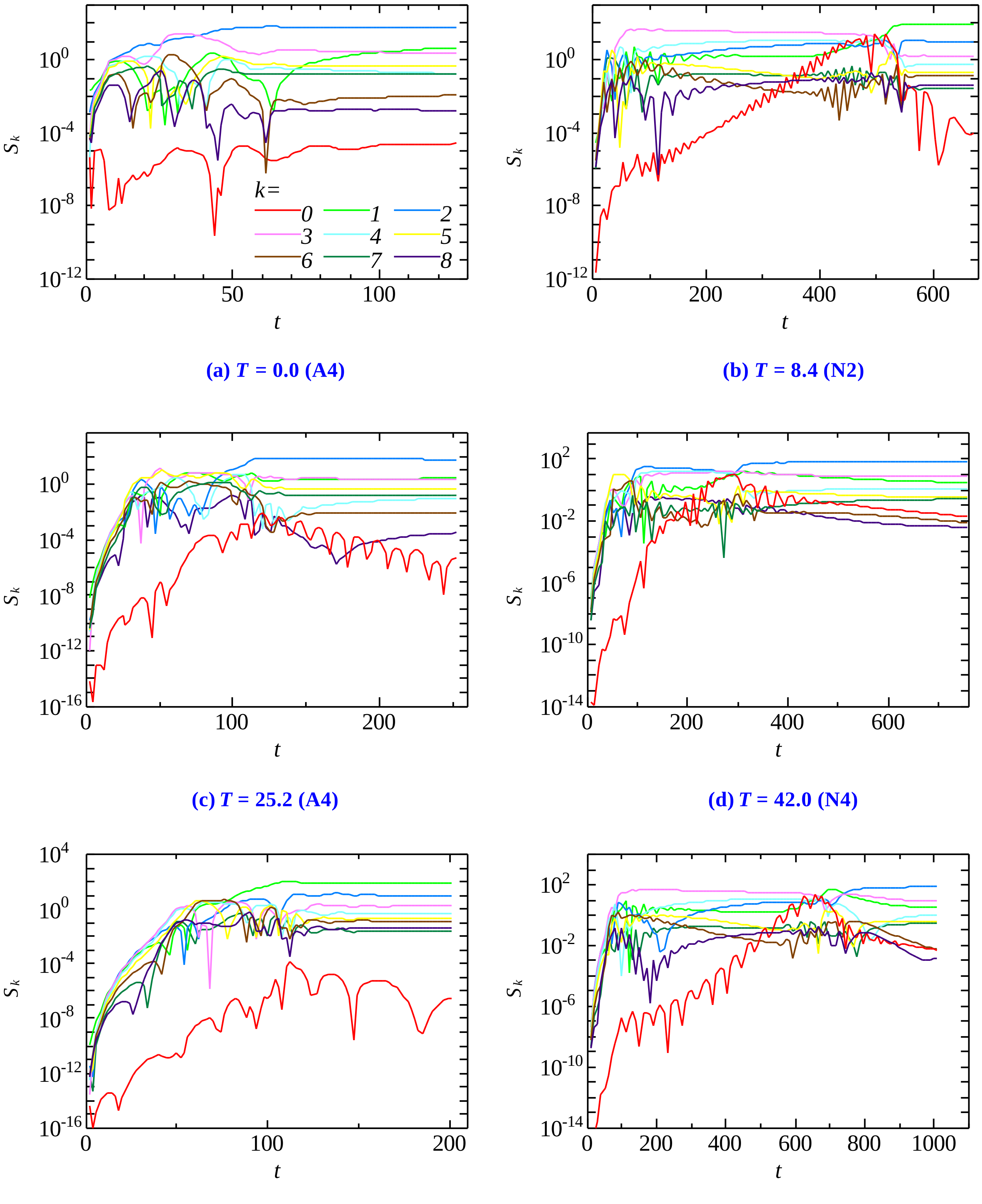

(a) *T* = 0.0 (A4) **(b) *T* = 8.4 (N2)**

(c) *T* = 25.2 (A4) **(d) *T* = 42.0 (N4)**

(e) *T* = 58.8 (N2) **(f) *T* = 84.0 (N4)**

Fig. 2. Time variations of S_k (? = 4.0, *Re* = 700).

Figure 2 (b) shows the time variation of S_k in the mode formation process of the normal two-cell mode. The final dominant wave number is one, and the final flow field has two vortices. Figure 2 (c), (d), (e) and (f) show the variation in the formation processes of the anomalous four-cell mode, the normal four-cell mode, the normal two-cell mode and the normal four-cell mode, respectively. The final mode has four, four, two and four vortices, respectively.

T	0.0	12.0	24.0	36.0	48.0	60.0	72.0	84.0	96.0	108.0	120.0
Mode	A5	A4	A6	N6	A4	N6	N6	N6	N4	N4	N6
E	0.07260	0.07058	0.07815	0.07183	0.07058	0.07190	0.07181	0.07182	0.07527	0.07527	0.07195
Ω	0.4961	0.4202	0.4784	0.5241	0.4202	0.5287	0.5240	0.5241	0.5077	0.5077	0.5270

Table 3. Final modes of the Taylor vortex flow (? = 4.8, *Re* = 1000).

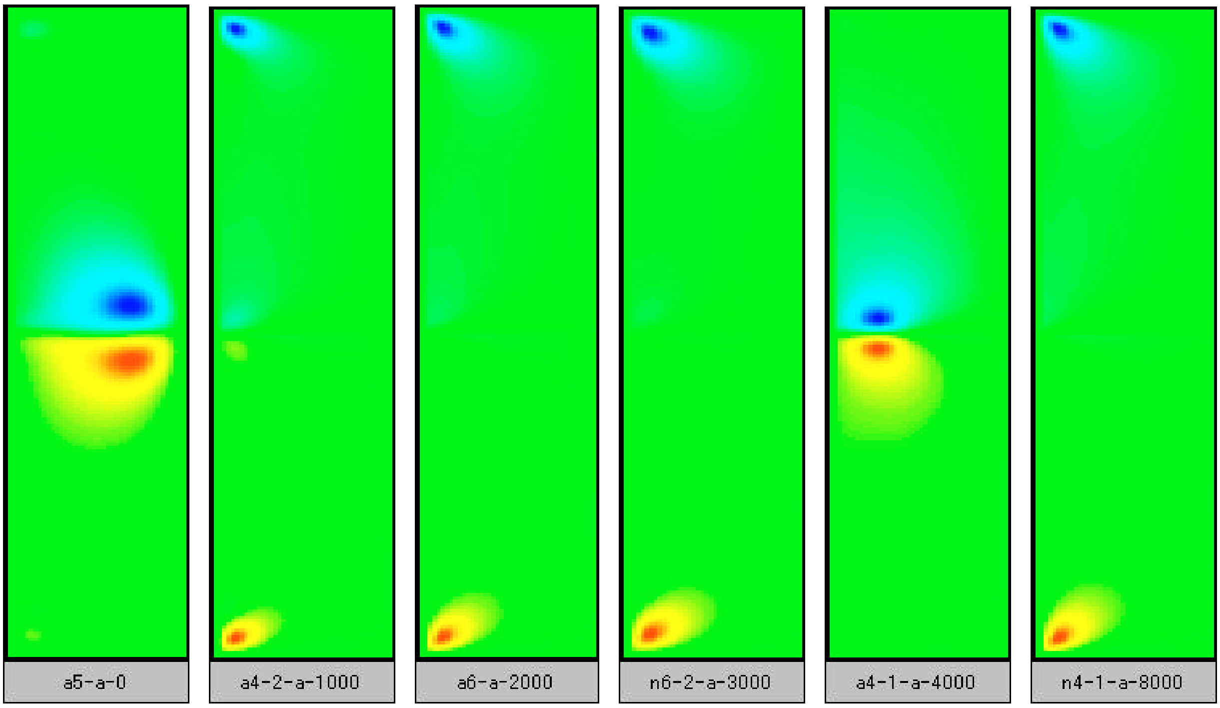

(a) *T* = 0.0 (A5) (b) *T* = 12.0 (A4) (c) *T* = 24.0 (A6) (d) *T* = 36.0 (N6) (e) *T* = 48.0 (A4) (f) *T* = 96.0 (N4)

Fig. 3. Mode formation process (? = 4.8, *Re* = 1000).
Double click each figure, and see animation.

Mode	Process	Mode	Process	Mode	Process
(b) A4 (T = 12.0)	N10→A8→A4	(a) A5 (T = 0.0)	N10→A8→A5	(d) N6 (T = 36.0)	N10→N6
(e) A4 (T = 48.0)	N6→A4	(c) A6 (T = 24.0)	A8→A6	(f) N4 (T = 96.0)	N10→N4

Table 4. The modes formation process of the Taylor vortex flow (? = 4.8, *Re* = 1000).

3.2 Mode formation process at ? = 4.8 and *Re* = 1000

Table 3 presents the mode formation processes at ? = 4.8 and *Re* = 1000. Depending on the acceleration rate of the inner cylinder, the flow has five different modes: the anomalous five-cell mode (A5), the anomalous four-cell mode (A4), the anomalous six-cell mode (A6), the normal six-cell mode (N6) and the normal four-cell mode (N4). At ? = 4.8 and *Re* = 1000, the non-uniqueness of the Taylor vortex flow is found, as is seen at ? = 4.0 and *Re* = 700. The normal six-cell modes are not stable, and their kinetic energy and mean enstrophy change with time. Figure 3 and 4 show the mode formation processes and the time variation of S_k, respectively.

Figure 3 (a) indicates the formation process of the anomalous five-cell mode. First, two vortices develop around the mid-plane, and the flow has the normal ten-cell mode. Next, the vortices attached to the end wall weaken and disappear, and the flow field has the anomalous eight-cell mode. Finally, the anomalous five-cell mode is formed. The time variations of the number of vortices are clearly found in Fig. 4 (a).

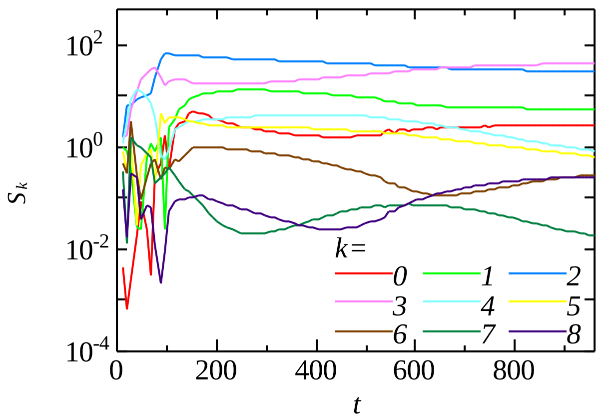

(a) T = 0.0 (A5)

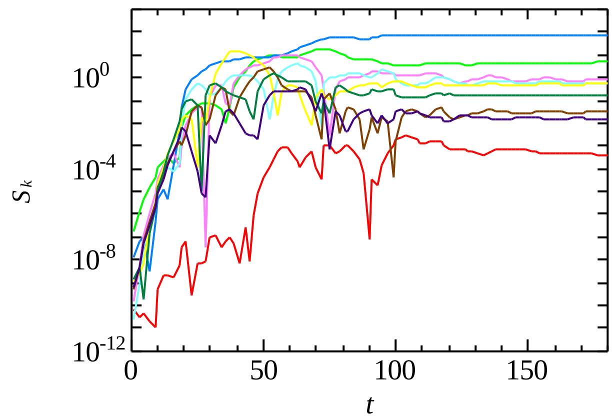

(b) T = 12.0 (A4)

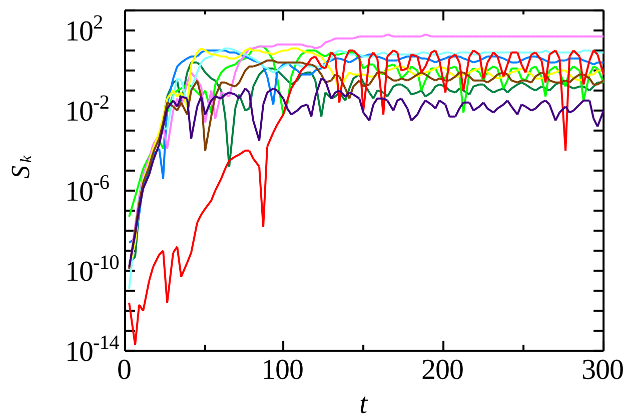

(c) T = 24.0 (A6)

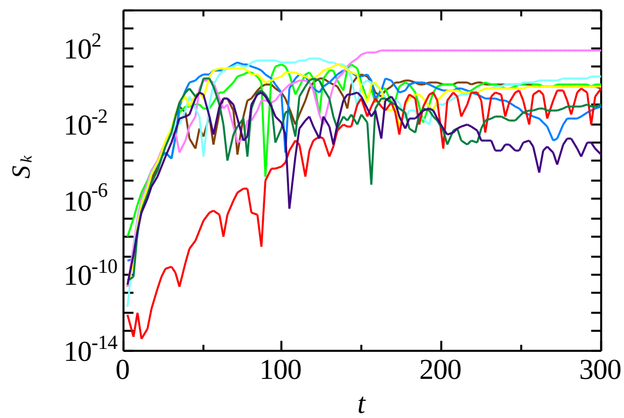

(d) T = 36.0 (N6)

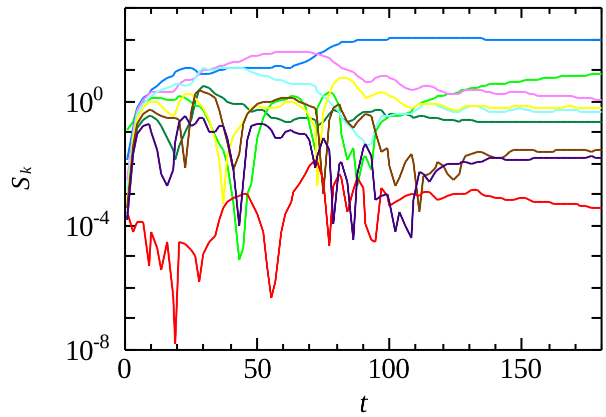

(e) T = 48.0 (A4)

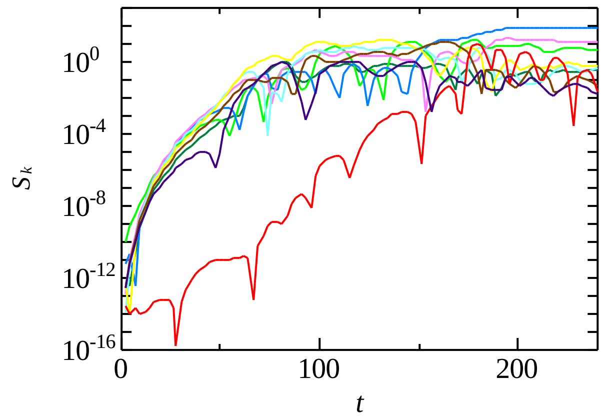

(f) T = 96.0 (N4)

Fig. 4. Time variation of S_k (? = 4.8, Re = 1000).

The formation processes shown in Fig. 3 are summarized in Table 4. In the formation processes of the anomalous mode, the second vortex divides the normal cell attaching to the cylinder end wall into the inner and the outer regions. The second vortices reach the cylinder end wall, and the flow field becomes the anomalous mode.

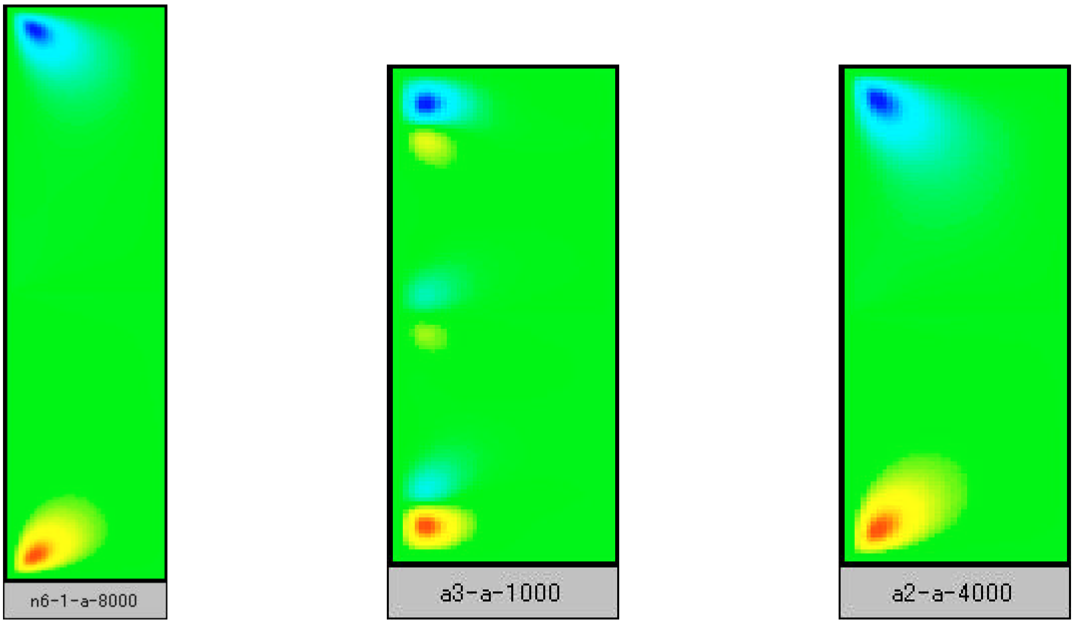

(a) ? = 4.8, *Re* = 300, *T* = 28.8 (N6) **(b) ? = 2.6, *Re* = 900, *T* = 10.8 (A3)** **(c) ? = 2.6, *Re* = 900, *T* = 43.2 (A2)**

Fig. 5 Mode formation process. Double click each figure, and see animation.

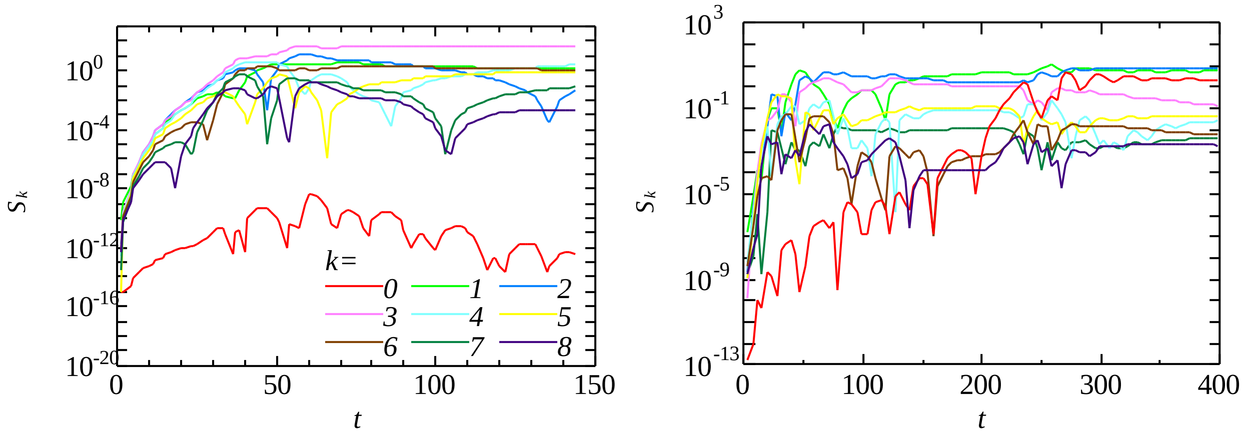

(a) ? = 4.8, *Re* = 300, *T* = 28.8 (N6) **(b) ? = 2.6, *Re* = 900, *T* = 10.8 (A3)**

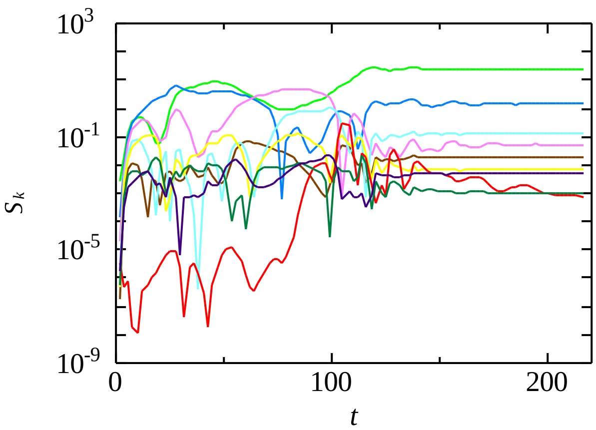

(c) ? = 2.6, *Re* = 900, *T* = 43.2 (A2)

Fig. 6 Time variation of S_k.

3.3 Mode formation process of N6, A3 and A2

Figure 5 and 6 show the flow developments and the time variation of S_k in the formation processes of the normal six-cell mode, the anomalous three-cell mode and the anomalous two-cell mode. Figure 5 (a) indicates the formation process of the normal six-cell mode. First, the two vortices develop at the inner-lower and the inner-upper corners, and the flow field has six vortices. The six vortices grow gradually, and the developed normal six-cell mode is formed. The time variation of S_k shown in Fig. 6 (a) indicates that the dominant wave number is 3 from the beginning of the mode formation process, and no mode change occurs.

Figure 5 (b) shows the formation process of the anomalous three-cell mode. In the first place, the vortices are generated around the mid-plane, and at the inner-lower and the inner-upper corners, and the flow field becomes the normal six-cell mode. Then, the flow field changes from the normal six-cell mode, via the anomalous four-cell mode, to the anomalous three-cell mode.
Figure 5 (c) presents the formation process of the anomalous two-cell mode. The flow field shifts from the six-cell mode, via the anomalous four-cell mode, to the anomalous two-cell mode.

4 DISCUSSION

At the beginning of the mode formation processes, there are two cases of the development of the vortices. In one case, the vortices develop around the mid-plane. In the other case, the vortices develop at the inner-lower and the inner-upper corners. In general, the vortices develop around the mid-plane at lower acceleration rate of the inner cylinder, and the vortices develop at the cylinder corners when the acceleration rate is larger.

In the mode formation processes described in Section 3.1, the normal two-cell mode is generated in two ways. In one way, the flow field changes from the normal six-cell mode to the normal two-cell mode (Fig. 1 (b)). In the other way, the flow field changes from the normal ten-cell mode to the normal two-cell mode (Fig. 1 (e)). Similarly, the anomalous four-cell mode (Fig. 1 (a) and (c)) and the normal four-cell mode (Fig. 1 (d) and (f)) have two different mode formation processes, respectively. Non-uniqueness of the Taylor vortex flow has been used to mean that the flow field has different modes at constant ? and *Re*. Now we find a new non-uniqueness of the Taylor vortex flow, which means that the mode formation processes are different even though the flow field has the same final mode. We can also find a new non-uniqueness in the formation processes mentioned in Section 3.2 (Fig. 3 (b) and (e).

Bielek et al. [9] experimentally concluded that the anomalous three-cell mode never formed directly after sudden start of the inner cylinder, but the mode originated from the decay of the anomalous four-cell mode or from the six-cell mode. In this study, the anomalous three-cell mode appears at $\Gamma = 2.6$, $Re = 900$ and $T = 10.8$. In this case, the flow mode shifts from the normal six-cell mode, to the anomalous four-cell mode, then to the anomalous three-cell mode. The result in this study agrees with Bielek et al.'s experimental observation.

At the fixed ? and *Re*, the order of the values of the mean enstrophy is listed as A2 < A3, A4 < A6 < N2 < N4 < N6. In general, the mean enstrophy of the normal mode is larger than that of the anomalous mode, and the larger number of vortices the flow field has, the larger the mean enstrophy is. However, some exceptions are found, for example, the enstrophy of the normal two-cell mode (N2) is less than that of the anomalous three-cell mode (A3). Therefore the relation of the mean enstrophy between modes is not concluded clearly. The relation of the mean kinetic energy between modes is not determined, neither.

5 CONCLUSIONS

The Taylor vortex flow between two concentric rotating cylinders with finite length has been investigated using the numerical flow visualization. The non-uniqueness of the Taylor vortex flow, which has been found in previous studies, is confirmed in the present study. Though the same final mode at constant ? and *Re* is formed, we found that the mode formation processes may be depend on the acceleration rates of the inner cylinder. That is, another modes may be taken during the flow development. At the same final mode, the mean kinetic energy is identical, and so is the mean enstrophy. The time variation of the power spectrums of the ψ integrated in the radial direction help us to determine the number of vortices quantitatively. The first vortices appear around the mid-plane as well as at the inner-lower and the inner-upper corners at the beginning of the mode formation, and the location depends on the acceleration rate of the inner cylinder. In the mode formation processes of the anomalous mode, the second vortex from the end wall divides the normal cell on the end wall into the inner and the outer regions of the annulus. Then, the second vortex reaches the cylinder end wall, and the anomalous mode is formed.

6 REFERENCES

[1] Benjamin T. B.: Bifurcation phenomena in steady flows in a viscous flow - II. Experiment-. *Proceedings of the Royal Society of London*, Series A, Vol. 359, pp. 27-43, 1979.

[2] Cliffe K.A.: Numerical calculation of two-cell and single cell Taylor flow. *Journal of Fluid Mechanics*, Vol. 135, pp. 219-233, 1983.

[3] Cliffe K. A.: Numerical calculation of the primary flow exchange process in the Taylor problem. *Journal of Fluid Mechanics*, Vol. 197, pp. 57-79, 1988.

[4] Bolstad J. H. and Keller H. B.: Computation of anomalous modes in the Taylor experiment. *Journal of computational Physics*, Vol. 69, pp. 230-251, 1987.

[5] Alziary de Roquefort, T. and Grillaud, G.: Computation of Taylor vortex flow by a transient implicit method. *Computers and Fluids*, Vol. 6, pp. 259-269, 1978.

[6] Lücke M., Mihelicic M. and Wingerath, K.: Flow in a small annulus between concentric cylinders. *Journal of Fluid Mechanics*. 140, pp. 343-353, 1984.

[7] Lücke M., Mihelcic M. and Wingerath, K.: Front propagation and pattern formation of Taylor vortices growing into unstable circular couette flow. *Physical Review*, A, Vol. 31, No. 1, pp. 396-409, 1985.

[8] Kuo D.C. and Ball K.S.: Taylor-Couette flow with buoyancy: onset of spiral flow. *Physics of Fluids*, Vol. 9, No. 10, pp. 2872-2884, 1997.

[9] Bielek C.A. and Koschmieder E.L.: Taylor vortices in short fluid columns with large radius ratio. *Physics of Fluids*, A 2-9, pp. 1557-1563, 1990.

[10] Watanabe T., Furukawa H., Aoki M. and Nakamura I.: Visualization of sudden-start flow between two concentric rotating cylinders. *Proc. 9th Int. Symp. Flow Visualization (this volume)*.